Soft Matter

Spatiotemporal Mapping of Nanotopography and Thickness Transitions of Ultrathin Foam Films

Journal:	*Soft Matter*
Manuscript ID	SM-TRV-01-2024-000048.R1
Article Type:	Tutorial Review
Date Submitted by the Author:	31-Mar-2024
Complete List of Authors:	Xu, Chenxian; University of Illinois Chicago, Chemical Engineering Zhang, Yiran; University of Illinois Chicago, Chemical Engineering Sharma, Vivek; University of Illinois Chicago, Chemical Engineering

Spatiotemporal Mapping of Nanotopography and Thickness Transitions of Ultrathin Foam Films

Chenxian Xu, Yiran Zhang, and Vivek Sharma*

Department of Chemical Engineering, University of Illinois Chicago, Chicago, IL.

*Address correspondence to: viveks@uic.edu

Submitted on:ohne January 12, 2024, Revised on March 26, 2024.

Abstract Freshly formed soap films, soap bubbles, or foam films display iridescent colors due to thin film interference that changes as squeeze flow drives drainage and a steady decrease in film thickness. Ultrathin (thickness < 100 nm) freestanding films of soft matter containing micelles, particles, polyelectrolyte-surfactant complexes, or other supramolecular structures or phases display drainage via stratification. A fascinating array of thickness variations and transitions, including stepwise thinning and coexistence of thick-thin flat regions, arise in micellar foam films that undergo drainage via stratification. In this tutorial, we describe the interferometry digital imaging optical microscopy (IDIOM) protocols that combine the conventional interferometry principle with digital filtration and image analysis to obtain nanometer accuracy for thickness determination while having high spatial and temporal resolution. We provide fully executable image analysis codes and algorithms for the analysis of nanotopography and summarize some of the unique insights obtained for stratified micellar foam films.

Introduction

Bubbles and films created using pure liquids like water drain and burst quickly, whereas soap bubbles and soap films have a relatively prolonged, dynamically richer, colorful existence and death.[1-5] Iridescent colors of a freshly prepared soap bubble or foam (freestanding) film under white light source illumination arise due to thin film interference.[1] The same phenomena are responsible for the structural color of many butterflies like *Papilio Palinarus*, oil slicks on rainy days, and multilayered polymer films.[6, 7] The iridescent colors disappear for ultrathin films (thickness, $h < 100$ nm). However, the thickness-dependent variation in interference intensity is manifested as soapy shades of gray ranging from whitish gray to black.[1, 2, 5, 8-10] Drainage of liquid away from foam films into the surrounding Plateau borders in foams and to meniscus in the thin film balance (Scheludko cell) is driven by the gradient in capillary or Laplace pressure, $P_c = \Gamma K$, which depends on surface tension, Γ and the curvature, K of the gas-liquid interfaces.[5, 11] Quantitative understanding and analysis of the spatial and temporal variation in thickness of ultrathin foam films are of immense practical importance for at least two reasons. Firstly, film drainage and rupture influence the stability, properties, and applications of foams which contain gas pockets separated by thin films.[1, 2, 4, 5, 12-15] Secondly, ultrathin films provide experimental and theoretical systems for observing the influence of colloidal forces or the intermolecular and surface forces that contribute thickness-dependent disjoining pressure, $\Pi(h)$ on drainage kinetics, nanotopography, and stabilization against rupture (extending foam stability) of ultrathin films.[5, 9, 16-24]

The observation of iridescent colors and black films by Hooke, first and later by Newton, prompted them to expound on the nature of light and soap films.[1, 2, 4, 5, 13, 14, 25] A galaxy of scientists have contributed to understanding interfacial tension, surfactant science, lubrication flows, and optics relevant to soap film studies.[2, 10, 14, 25-27]

Experiments established the existence of two distinct blacks in ultrathin foam films and postulated that the two thicknesses are set by intermolecular distances and forces by the end of the nineteenth century, even though the existence of molecules or molecular hypothesis was controversial.[25, 28, 29] In 1906, Johonnott reported the existence of multiple blacks (as many as five).[29] A decade later, Perrin observed stepwise thinning, with similar size steps that he assumed to be characteristic of a molecular size.[30, 31] Perrin cited stratification (also probably coined the term in this context) as additional evidence for molecular reality in 1926 in his Nobel lecture.[30, 31] The fragile, transient nature of soap films that inspired curiosity-driven quests into the nature of light and matter, fascinates children, painters, poets and scientists alike,[1, 2, 5, 14, 32-35] Foam films or soap films have continued to serve as model systems for characterizing the influence of intermolecular and forces, interfacial adsorption, self-assembly, free-surface flows, and 2D turbulence.[3, 13, 27, 35-37] Foam films contain interfacially active amphiphilic molecules or surfactants spontaneously adsorbed to liquid-air or oil-water interfaces. The adsorbed surfactants reduce surface tension, aiding in the creation of new surfaces, and therefore act as foaming or emulsifying agents. The amphiphilic molecules self-assemble in aqueous dispersions to form supramolecular micelles above a critical micelle concentration (CMC).[38] For small molecule surfactants, surface tension, Γ attains a nearly constant value for $c >$ CMC (critical micellar concentration).[11] For ionic surfactants, the two blacks, common black film (CBF, $h < 20$ nm) and Newton black film (NBF, $h \sim$ few nm), manifest for $c <$ CMC,[5, 10, 14, 16, 17] whereas $c >$ CMC, foam films display step-wise thinning with the appearance of coexisting flat regions with multiple quantized thicknesses that appear as coexisting shades of gray.[8-10, 18-24, 39-46]

It is well-established now that the multiple blacks or progressively darker shades of gray for freely draining micellar foam films arise due to a supramolecular

oscillatory structural force contribution to disjoining pressure, $\Pi_{os}(h)$ that is attributed to confinement-induced layering of micelles.[8, 9, 17-24, 41-45] The experimental characterization of the thickness variations and transitions is a critical step towards developing a deeper understanding of the stratification dynamics and the role played by capillary and disjoining pressure. Extensive literature describes the creation and evolution of the nanotopography of supported films undergoing dewetting under the influence of capillarity and surface forces.[11, 47-53] However, mapping nanoscopic thickness evolution and variations in freestanding films, including stratifying micellar foam films, was a long-standing challenge.

Typical foam film drainage studies obtain an average film thickness as a function of time using the electrical (involving resistance/conductance measurement), or optical techniques, including spectroscopy and interferometry.[1, 5, 14-17, 44, 45, 54-61] Among these, interferometry is the most used most commonly as it allows non-intrusive, nanometer accuracy thickness measurement. A beam of light incident upon a thin film undergoes multiple reflections at the upper and lower interfaces. Therefore, the reflected light intensity is determined by interference between a series of reflected lights with diminishing amplitude, influenced by film thickness, h and refractive index, n. Traditional interferometry illuminates a thin film with monochromatic light from a laser or filtered light as the source and uses a photodiode to measure the reflected light intensity and the temporal evolution of a local film thickness from the chosen region of interest. The light intensity reflected from a spot size of 1-100 μm is tracked over time using a photodetector to obtain $I(t)$, and it is converted into the temporal evolution of the average thickness within the sampling spot.[34, 44, 45, 54, 62] However, these measurements lack the spatial resolution for studying dynamics and pattern formation in stratifying foam films.

In 2015, Zhang and Sharma developed their Interferometry Digital Imaging Optical Microscopy (IDIOM) protocols by combining the white light illumination and pixel-wise detection of reflected intensity using a digital camera.[8, 9] The IDIOM protocols facilitate mapping of the nanoscopic thickness transitions of foam films with exquisite spatiotemporal resolution (thickness < 10 nm, lateral < 1 μm, temporal < 1 ms). Though the IDIOM protocols have been used for visualizing and analyzing the nanotopography of the stratifying micellar foam films extensively in studies published from this research group[8, 9, 18-24, 63-66] and a countable few others,[67-69] the method has not been adopted by a wider community possibly due to the extra effort needed for compiling image analysis protocols and understanding the physical basis for the nanotopographical analysis.

In this tutorial, we present a comprehensive examination of the IDIOM protocols. We illustrate the approach pedagogically and supplement the text with a complete set of MATLAB scripts with examples and annotations to enable a seamless adoption by foam formulators and researchers. The tutorial discusses the challenges of picking a representative region of interest for examining step-wise thinning from plots of average thickness *vs.* time. We include a movie of a stratifying foam film that corresponds to the grayscale images and reconstructed thickness maps that show nanotopographical features, including nanoridges and mesas. The tutorial illustrates the physical principles underlying interferometry-based mapping of nanotopography and summarizes the physicochemical processes underlying the drainage of micellar foam films.

Interferometry Digital Imaging Optical Microscopy (IDIOM) Protocols

Drainage and stratification of a single horizontal micellar thin film is visualized and characterized with the thin film apparatus and imaging system shown schematically

in Figure 1. A circular thin film with nearly plane-parallel gas-liquid interfaces is formed at the center of the cell, and a syringe pump is used to control the fluid volume in the cell. The film is surrounded by a thicker meniscus, analogous to the Plateau border in real foams. The Scheludko-like cell is placed within a closed chamber containing the same surfactant solution used in experiments to minimize the effect of evaporation. The cell consists of a miniature glass cylinder (inside diameter, d_c = 1.6 mm) with a small orifice (< 0.1 mm) drilled on the side wall and a stainless-steel needle fixed in the orifice to connect liquid in the cell to a syringe pump (New Era NE-1000). The test solution is loaded into the cell to form a biconcave drop. A circular thin film is formed by slowly withdrawing liquid from the drop using the syringe pump. Once the desired film diameter, d_f is reached, the withdrawal is stopped to maintain a constant fluid volume throughout the film drainage process.

The capillary pressure difference between the plane-parallel thin film and the curved Plateau border drives the drainage. This capillary pressure difference, P_c can be estimated by assuming that the surfactant solution completely wets the glass cell wall, and the contact angle between the thin film and the Plateau border is small. Therefore, P_c is given by:

$$P_c \approx \frac{4\Gamma d_c}{d_c^2 - d_f^2} \qquad (1)$$

where Γ is the surface tension of the test solution. It has been suggested that the kinetics of stratification is influenced by the size of the film.[22, 23, 39, 44, 45, 70] As a result, we suggest maintaining the initial size of the film (d_f = ~300 μm) across experiments with different surfactant concentrations, to make meaningful comparisons. The initial capillary pressure in the experiments described in this study is around 90 Pa. At a later stage of the film drainage, the film reaches small thicknesses, and the micellar structural disjoining pressure becomes large enough to completely balance the driving capillary

pressure and bring the drainage to a halt. Further stepwise thinning can be induced by withdrawing more liquid and increasing d_f. In an alternative protocol used by Anachkov et al.,[42] the cell container is opened briefly to allow evaporation, which results in an increase in the capillary pressure and consequently in a step transition.

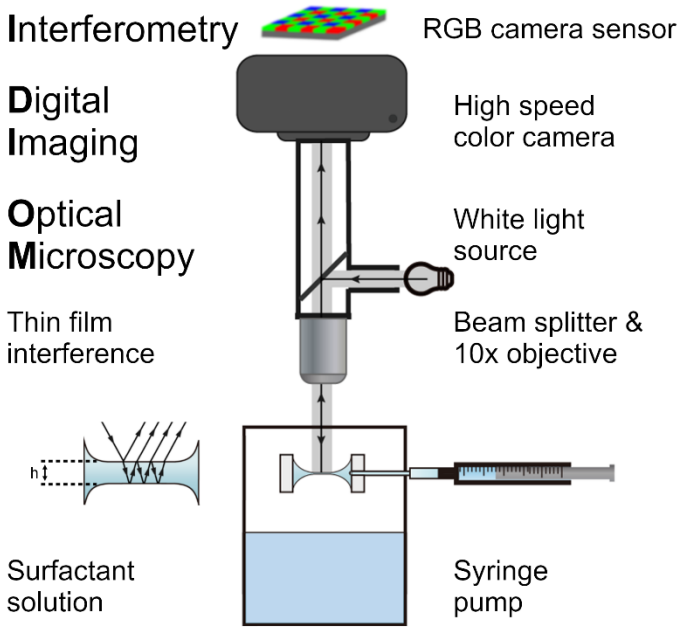

Figure 1 Schematic of the setup used for Interferometry Digital Imaging Optical Microscopy (IDIOM) protocols. A single foam film is created in a cell placed in a closed container, and the film undergoing drainage is visualized using reflected light microscopy. The plane-parallel film and surrounding meniscus in this Scheludko-like cell emulate a single foam film in contact with Plateau borders. The syringe mounted on a syringe pump is used to pump in a finite volume of fluid using the side arm and then to withdraw slowly till the plane-parallel film reaches a thickness where the last interference fringes disappear. No liquid is added or withdrawn during the drainage experiment, so ensure free and spontaneous drainage from the film into the meniscus. Spatio-temporal variation in interference intensity $I(x, y, \lambda, t)$ of the reflected light is extracted from RAW images and used for computing the effective thickness of the foam film with in-plane resolution set by microscopy.

The drainage process of the single horizontal micellar thin films formed in the thin film apparatus is captured as RAW format images/videos (12-bit depth) by a reflected light microscope. The imaging system consists of precision microscope lens system (Navitar Zoom 6000 with a 10x microscope objective), and a high-resolution, high-speed color camera (FASTCAM Mini UX100) with high-quality CMOS or CCD

sensors (See Figure 1). The illumination is provided by a white LED light source (Fiilex P360EX) with adjustable color temperature (set to 5100K for most experiments). The protocol of IDIOM, as described above, was tested with various other cameras and illumination light sources by Zhang *et al*. in 2016.[9]

Following Sheludko,[34] for a freestanding homogeneous flat film with identical interfaces in which light adsorption can be neglected and for a nearly perpendicular incident beam of monochromic light, a relatively accurate measure of film thickness, h can be obtained from the function of a normalized measure of intensity, $\Delta = \left(I - I_{\min}\right)/\left(I_{\max} - I_{\min}\right)$, that minimizes the influence of source intensity and background/detector errors:

$$h = \frac{\lambda}{2\pi n}\arcsin\left(m\pi \pm \sqrt{\frac{\Delta}{1+4R\left(1-\Delta\right)/\left(1-R\right)^2}}\right) \tag{2}$$

Here, n is the refractive index of the thin film, $R = (n\text{-}1)^2/(n+1)^2$ is the Fresnel coefficient of the film interface, λ is the wavelength of the incident light, $I_{\max}$ and $I_{\min}$ are maxima and minima intensities of the last order of interference. The derivation is shown in the Appendix. For thicker films (h ~ 0.1-1 μm), the film thickness can be determined once the interference order, m, is known. For thinner films (h < 100 nm), the entire visible wavelength range corresponds to m = 0, and colorless (gray or black) film under white light illumination shows the influence of thickness variation. As the IDIOM protocols use the photodetector array of a digital camera, pixel-wise characterization of intensity is possible and thickness maps have an in-plane spatial resolution comparable to optical microscopy. The experiments described here are conducted with horizontal films, for the presence of any tilt is accompanied by the rising of thinning regions, sinking of thicker regions, and additional flows attributed to marginal regeneration.[2, 5, 71, 72] We used IDIOM protocols to characterize spinodal

stratification in vertical foam films,[19] and described how regions are advected in response of stresses contributed by of buoyancy, gravity, and capillarity.

Example of Drainage via Stratification in Micellar Foam Films

Figure 2 shows a montage of a stratifying SDS micellar thin film with c_{SDS} = 90 mM captured by IDIOM protocols. The stratifying thin film shows five coexisting shades of gray, which represent five coexisting thick-thin regions (marked as h_0 to h_4). Stratification occurs through nucleation and expansion of thinner, darker circular domains in thicker, brighter surrounding thin film. Rich and complex patterns can be observed, including faint halos and white spots formed around the expanding darker domains.

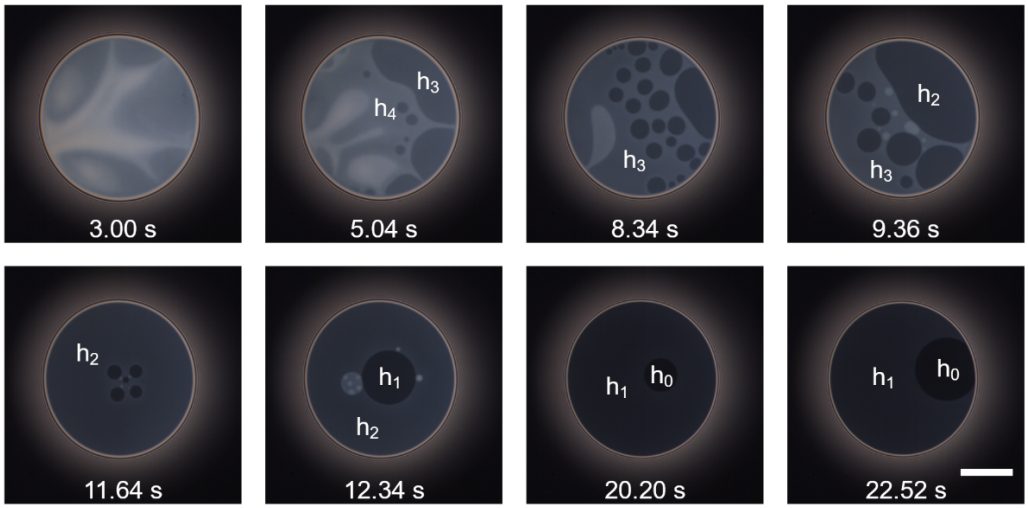

Figure 2 Montage of a stratifying SDS micellar thin film with c_{SDS} = 90 mM. The image sequence was captured using the IDIOM setup. Five thickness transitions are observed; each gray shade represents a distinct thickness (h_0 to h_5). The scale bar represents 100 μm.

The characterization and analysis of the thickness variations and transitions in stratifying foam films with a high spatiotemporal resolution by IDIOM protocols follow the following algorithm. Drainage of a thin freestanding is examined using the set-up shown schematically in Figure 1. Color images captured using a high-quality CMOS or

CCD sensor of a high-speed digital camera in the RAW format provide pixel-wise intensity maps for three wavelengths, $I(x,y,t,\lambda)$. Three images corresponding to red, green, or blue wavelengths are generated using digital filtering. After that, the intensity of each pixel at each instant or for each snapshot is used to compute thickness using equation 2. Thus, the images can be converted into thickness maps $h(x,y,t)$ from three color channels, and in the absence of absorption, all three provide similar measurements. These three values are then averaged to reduce noise. Although a color camera is used in the current setup, pixel-wise intensity obtained from a monochromatic digital camera can be used to determine thickness variation, implying that a color camera is not necessary for carrying out thickness mapping using the IDIOM protocols.[9]

Figure 3a shows a RAW format color image of the stratifying thin film at 11.64 s. The image is loaded as a three-dimensional matrix in which each image pixel contains three values associated with the light intensities of red (wavelength, λ = 600 nm), green (λ = 546 nm), and blue (λ = 470 nm) lights. The light intensity recorded in each color channel is represented as a value in the range of 0-4095 (12-bit depth for the specific camera used). The specially developed codes based on Equation (2) with m = 0 (included as supplementary files online), the light intensity of each pixel can be converted into thickness for each color channel in MATLAB R2016a. The thickness determined from Equation (2) with m = 0 is a measure of "equivalent film thickness", assuming the bulk solvent refractive index for the entire thin film, even though the two interfaces are surfactant enriched. An alternative three-layer model uses different refractive indices for the adsorbed surfactant layers and the aqueous solution in between.[44, 57] However, if appropriate values for thickness and refractive index of the adsorbed layer are obtained, the correction introduced by the model turns out to be negligible for SDS films.[44] For the dilute surfactant solutions used in this study, water

refractive index is used, n = 1.33. Equation (2) with m = 0 also neglects visible light absorption, includes multiple reflections within the film, assumes a near normal incidence, and considers only zeroth order of interference, which are valid assumptions for films with thickness $h < \lambda/2\pi n$ (h < 85 nm for the shortest blue wavelength).

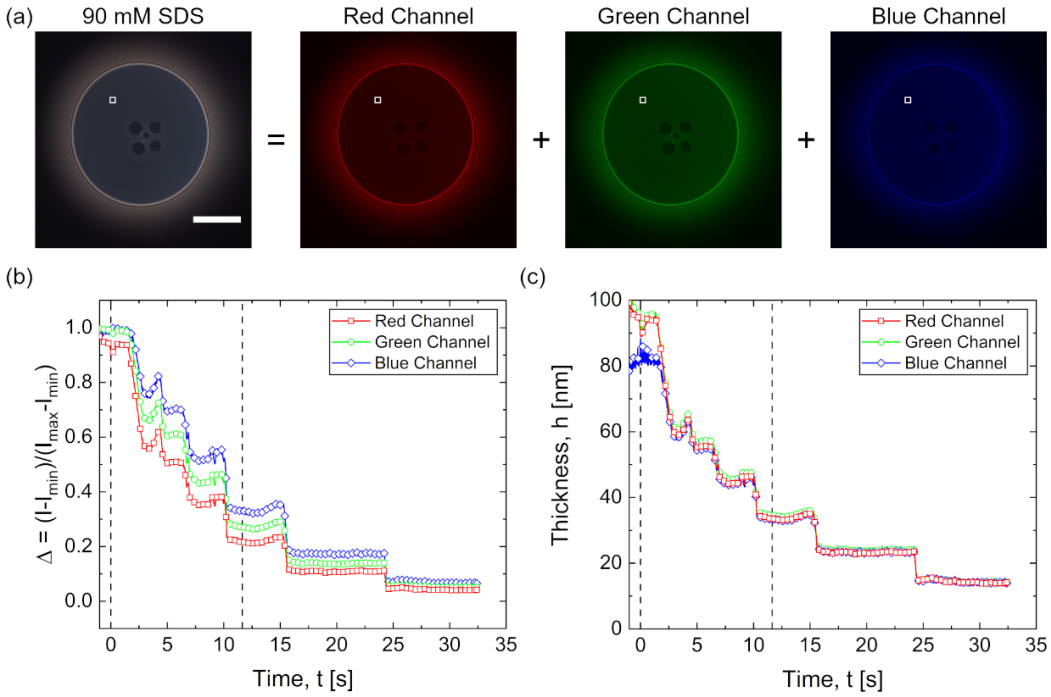

Figure 3 Average thickness *vs.* time plot of a fixed sample square region on a stratifying SDS micellar thin film with c_{SDS} = 90 mM. (a) Snapshot of the thin film at 11.64 s. The image is split into three channels (red, green, and blue with λ = 600, 546, 470 nm). The onset time, t = 0 s, is defined as the instant when the zeroth order interference is reached for the blue light (with the shortest wavelength). The scale bar represents 100 μm. (b) The normalized intensity *vs.* time plot of the sample region is marked by the small white box with a 25-pixel side length, shown in Figure 3a. The intensities extracted from the three-color channels are presented with the corresponding colors. The first dashed line labels the instant, t = 0 s, and the second dashed line labels the instant, t = 11.64 s. (c) Average thickness *vs.* time plot of sample region. The thickness extracted from the three-color channels are presented with the corresponding colors.

The value of I_{max} is determined by tracking the intensity over time and finding its last maxima, which corresponds to a bright white color in the images and a film thickness of $\lambda/4$, which tends to be 117.5 nm, 136.5 nm, and 150 nm for the blue, green and red channel, respectively. The minimum intensity in zeroth order interference, I_{min},

reaches zero film thickness. After each experiment, the thin film apparatus is removed from the field of view and the background intensity is recorded as I_{min}. Care is taken to avoid stray reflections from the apparatus and the container. The gas-liquid interface of the surfactant solution in the closed container is always kept out of focus to avoid reflection (distance from the thin film > 10 cm, 10 times focal length).

To mimic the conventional interferometry methods, the film thickness evolution over time and step-sizes are calculated by taking an average of the normalized intensity in a square sample region with a side length of 25 pixels. This procedure is typically repeated several times at different regions within the thin film area to ensure the values obtained are not affected by inhomogeneity in film thickness (and light intensity) or any tilt in horizontal films. Figure 3b shows the plot of the scaled intensity ratio against time for each of the three channels or wavelengths. The scaled intensity decreases in a stepwise fashion for all three wavelengths. The plot echoes or emulates the intensity-time plots shown in some studies in lieu of actual thickness-time plots.[70, 73] Figure 3c shows the thickness-time plot or film thickness evolution over time computed using Equation (2) for each wavelength and each snapshot. After the onset time, $t = 0$ s, thickness measurement following Equation (2) with $m = 0$ becomes valid, and the thicknesses measured from three color channels (plotted in their respective colors) are almost identical. The differences between them are typically < 1 nm. Figure 3c shows that the film thins in a step-wise fashion, with multiple thickness steps corresponding to different shades of gray observed in the snapshots (included in Figure 2). Figure 3a shows one snapshot at $t = 11.64$ s, where the two shades co-exist and correspond to one of the thickness steps. The transition from thicker to thinner step in the average thickness *vs.* time plot (Figure 3c) occurs when the thinner part of the film grows into and occupies the sample region. The step heights between thickness transitions, $\Delta h = h_n - h_{n-1}$, remain almost constant throughout the stratification.

Nevertheless, Figure 3c shows the time evolution of thickness during drainage, obtained by analyzing the average reflected light intensity of a single, fixed location, the region of interest, in the lab frame. The montages included in Figure 2, and the corresponding video (supplementary video online) illustrate that the spontaneous formation, growth, coalescence, and motion of darker (thinner) domains or brighter (thicker) white spots (we call mesas[8, 22, 23]) influences the instantaneous value of thickness measured. Though the gross thickness-time plot shows stepwise thinning with consistent step size, the duration for which a particular step thickness is registered in plots like Figure 3c varies based on the size and location of the chosen region of interest. Furthermore, the thickness-time plots provide no information about the considerable variation in the number, shape, and size of domains and mesas formed at any instant as film thickness decreases in a stepwise manner. Most significantly, characterization of the formation and evolution of the complex thick-thin patterns is necessary for developing a better understanding of the physicochemical processes that drive drainage by stratification.

Nanotopographical mapping of stratified micellar foam films

Figure 4 shows the nanotopography of the stratifying foam films obtained from IDIOM protocols such that the thickness maps correspond to the grey scale images included in Figure 2. The thickness maps facilitate a high-resolution visualization of the nanotopographical features formed as micellar foam film undergoes drainage via stratification. The mapping enables a detailed investigation of the complex patterns formed by the coexisting thick-thin regions and shows non-flat structures, including ridges formed between relatively flat regions. Even though a faint halo can be visualized around an expanding domain in grey-scale images, thickness maps enable quantitative analysis of the shape evolution of nanoscopic ridges formed at the moving front between the expanding domain and thicker surroundings. As the thickness difference between the non-flat nanoridge and the relatively flat region of the

surrounding is small (only a few nm), and the expansion of domains changes the location of ridges in a film, attempting to characterize such variations with conventional interferometry is futile. In the early 1990s, tracking the growth of individual isolated thinner, darker domains revealed a growth law of $R \propto t^{1/2}$ that was attributed to the diffusion of micelles and vacancies in the "ordered colloidal crystal" mechanism by Nikolov, Wasan, and collaborators.[39-41, 70, 74] In contrast, a hydrodynamic mechanism using a thin film equation was proposed by Bergeron and Radke,[45] and also utilized by Langevin and coworkers,[75] postulating that the rapid removal of fluid from the domain region leads to the formation of nanoscopic ridge around growing domains. However, in the absence of thickness mapping, the existence of the ridge itself and the mechanism driving stratification remained unresolved till we developed the IDIOM protocols.[8, 9, 19, 22]

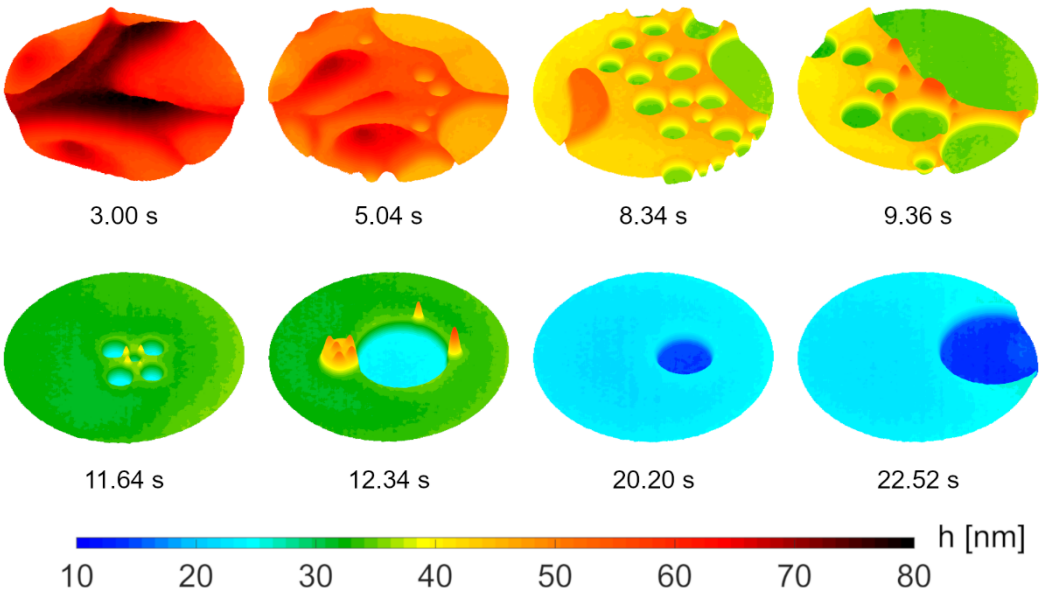

Figure 4 Thickness maps obtained using IDIOM protocols. The maps correspond to the snapshot of freely draining thin film shown in Figure 2. The exquisite spatiotemporal resolution (thickness < 10 nm, lateral < 1 μm, temporal < 1 ms) of these thickness maps enables visualization of five-layer coexisting thick-thin flat regions and the nonflat nanoscopic structures formed between these regions.

The detailed shape, thickness profile, and evolution of the nanoridge were characterized experimentally for the first time by IDIOM protocols in 2018 by Zhang

and Sharma[22]. The nanoridge shape radially outwards from a growing domain includes an inner region adjacent to the thinner domain, the peak, and an outer region that merges with the thicker surrounding film. The experiments show that the inner nanoridge region adjacent to the thinner domain displays a quasistatic shape, stationary in the frame, that travels with the domain expansion rate. The nanoridge peak grows vertically over time, whereas the outer region displays a self-similar shape captured by a similarity variable containing a ratio of radial distance to the square root of time. We further showed that the nanotopography evolution can be described using the thin film equation amended with supramolecular oscillatory structural disjoining pressure.[8, 9, 19, 22]

The nanoridge can undergo topological instability, forming mesas (white spots) around the domain, as visualized in the second row of Figure 4. As the thickness scale is in nanometers while the in-plane length scale is in micrometers, the brighter, white spots have a pancake-like shape so that they are regarded as mesas (see thickness maps at 9.36 s and 11.64 s in Figure 4). Moreover, the white spots with multiple layers can sometimes form (see thickness map at 12.34 s in Figure 4), often due to mesa coalescence. Zhang and Sharma[23] tracked the thickness evolution around expanding domains during the instability that led to the formation of mesas and argued that mesas form and grow due to a disjoining-pressure-driven instability. Thickness visualization shows that the nanoridge region between mesas retains its shape as mesas form and grow, implying that the observations were inconsistent with the mechanism of capillarity-driven Rayleigh-type instability advanced in the literature. Zhang and Sharma found that even though domain expansion kinetics display an initial growth law of $R \propto t^{1/2}$, the growth law changes to $R \propto t$ after mesas appear and domains coalesce with the Plateau border. So mechanistically, a combination of detailed analysis of the thin film equation and thickness maps obtained using IDIOM show that initially

apparent diffusive growth occurs due to restriction on the outward mass flux, and growth speeds up when mesas and Plateau borders act as reservoirs for material removed from growing domain region.

The examples in this manuscript (and our previous studies) represent fascinating early steps in unraveling the role of disjoining pressure in driving flows and sculpting the nanotopography of ultrathin film. In addition to characterizing the shape evolution of nanoridges and evaluating nanoridge-mesa instability, we have deployed IDIOM protocols to visualize and characterize spinodal stratification (the first observation in freestanding films),[19] the change in the appearance of isolated mesas in foams formed by salt-added micellar SDS solutions[18, 65] as well as in foams formed with bile salts.[64] We infer that ultrathin films provide an exquisite, frugal visual system for observing thermodynamics and hydrodynamics of confined supramolecular structures, their influence on colloidal forces or $\Pi(h)$, and macroscopic rheology and stability.[9, 17-21, 64, 65, 76] The stratification studies with IDIOM need to be supplemented by careful studies of adsorption kinetics and interfacial rheology that also influence dynamics and kinematics of foam formation, drainage, and rupture.[3, 5, 37, 58, 77, 78] We anticipate the completely executable list of codes included with this tutorial (included in supplementary files online and deposited to the GitHub repository[79])will provide the community with the toolbox needed for exploring detailed questions about the influence of the choice of surfactant and additives on nanotopography and drainage of thin films of soft matter.

Conclusion & Outlook

The tutorial details the experimental setup and image analysis codes that enable high-resolution nanoscopic thickness mapping of thickness variations and transitions in freestanding films by using the IDIOM (interferometry digital imaging optical

microscopy) protocols. We summarize how we utilized the IDIOM protocols to develop a better understanding of flows and fluxes that drive the drainage via stratification in micellar foam films made from aqueous SDS solutions. Several characteristic features of stratification are analyzed in this tutorial. The thickness evolution plots show stepwise thinning with discrete jumps in thickness. The coexisting thick-thin regions observed in reflected light as regions with distinct grey scale intensity are shown to have distinct nanoscopic thicknesses. Furthermore, the thickness maps show the existence of topological transitions that create non-flat structures like ridges and mesas. The noninvasive imaging and characterization of ridges, mesas, and terraces in freely standing thin films continue to revolutionize the study of nanoscale rheology and of surface and intermolecular forces, especially the understanding of non-DLVO, including supramolecular oscillatory surface forces that underlie stratification. We hope that the widespread use of IDIOM protocols will lead to a better understanding of interactions, flows, and self-assembly in biology, chemical physics, foams and colloidal science.

Acknowledgment

We acknowledge that many aspects of the set-up, code, and analysis for the IDIOM protocols were optimized over the last ten years through the inputs from several former and current students at UIC, including Subinur Kemal, Chrystian Ochoa, Yash Vidyasagar, Colin Pearsall, and William Yang, among others. We acknowledge the supplementary funds provided by the Dean and the College of Engineering at UIC for procuring the high-speed camera used in the set-up.

Appendix: Thin Film Interference

Consider a beam of monochromatic light of wavelength, λ incident onto a flat thin film (or plane parallel plate) of thickness, h and refractive index, n'. Consider the

surrounding and thin film media to be transparent and homogeneous, with the refractive index of the surrounding media as n. Suppose that a plane wave of this monochromatic, linearly polarized light is incident on the film interface at an angle, θ and reflection and refraction occur, following the standard laws of reflection and refraction (or Snell's law). For the light traveling from the surrounding to the thin film, the reflection and transmission coefficients are denoted as r and t, while for the light traveling from the thin film to the surrounding, the corresponding coefficients are denoted as r' and t'. The reflection coefficient (the amplitude ratio of reflected and incident light) and transmission coefficient (the amplitude ratio of refracted and incident light) quantify the change of light amplitude. The reflection and transmission coefficients can be calculated from Fresnel formulae, leading to $r = -r'$ and $r^2+tt' = 1$. With the definition of the reflectivity, $R = r^2 = r'^2$ and the transmissivity, $T = tt'$, $R+T = 1$. When a beam of light is incident on a thin film, multiple reflections and refraction can occur on both upper and lower interfaces (see Figure 5), and multiple-beam interference happens between a series of reflected lights with diminished amplitude (p = 1, 2, …).

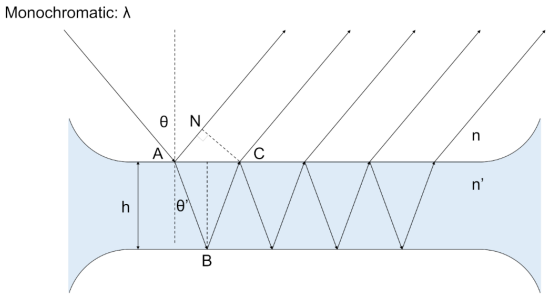

Figure 5 Schematic of thin film interference. Here the amplitude and intensity of the reflected light are determined by interference that occurs between multiple beams reflected at the two liquid-air interfaces. Refractive index, angle of incidence, and film thickness influence the total path or phase difference between wave that interfere.

The phase difference between p-th and (p+1)-th reflected light is:

$$\delta = \frac{2\pi n'}{\lambda}\left(|AB|+|BC|\right) - \frac{2\pi n}{\lambda}|AN| \tag{3}$$

Using the geometric relations shown in Figure 5, this phase difference correlates with the film thickness:

$$\delta = \frac{4\pi}{\lambda} n' h \cos\theta' \tag{4}$$

In the equation, θ' represents the angle of refraction, and the schematic as well as Equation (4) illustrate that phase difference changes with angle of incidence. Assuming negligible light adsorption within the thin film, the complex amplitude ratio of reflected light and incident light is shown to be r for $p = 1$ and $tt'r'^{(2p-3)}e^{i(p-1)\delta}$ for $p > 1$. The complex amplitude ratio obtained from the superposition of the first q reflected waves can be written as:

$$\begin{aligned} \frac{A_r(q)}{A_i} &= r + tt'r'e^{i\delta}\left[1 + r'^2 e^{i\delta} + \cdots + r'^{2(q-2)} e^{i(q-2)\delta}\right] \\ &= r + \left[\frac{1 - r'^{2(q-1)} e^{i(q-1)\delta}}{1 - r'^2 e^{i\delta}}\right] tt'r'e^{i\delta} \end{aligned} \tag{5}$$

For an extended thin film, the number of reflected waves is large and in this limit of q going to infinity, the amplitude ratio becomes:

$$\frac{A_r}{A_i} = \frac{A_r(\infty)}{A_i} = -\frac{r'\left[1 - \left(r'^2 + tt'\right)e^{i\delta}\right]}{1 - r'^2 e^{i\delta}} = \frac{\sqrt{R}\left(1 - e^{i\delta}\right)}{1 - Re^{i\delta}} \tag{6}$$

Thus, the intensity of the reflected light, $I = A_r A_r^*$ follows the Airy's formula:

$$\frac{I}{I_0} = \frac{4R\sin^2\frac{\delta}{2}}{(1-R)^2 + 4R\sin^2\frac{\delta}{2}} \tag{7}$$

In this equation, I_0 represents the light intensity of the incident light. The reflected light intensity I can be correlated with the film thickness, h after combining with the Equation (4). Since the phase difference also depends on the angle of incidence, interference intensity changes with change in viewing angle, leading to iridescence.

In 1967, Sheludko[34] summarized an alternative formula for carrying out foam film thickness analysis without the need for characterizing the absolute value of incident light intensity, I_0. Instead of using I/I_0, the formula relates the phase difference, δ to the normalized intensity $\Delta = \frac{I - I_{\min}}{I_{\max} - I_{\min}}$. Here, $I_{\min}$ represents the background intensity (including noise) with a relatively small value so that practically $\Delta \approx I / I_{\max}$. The maximum intensity, $I_{\max} = \frac{4R}{(1-R)^2 + 4R}$ is reached for $\sin\frac{\delta}{2} = 1$. Thus, the normalized intensity can be written as:

$$\Delta = \frac{\left[(1-R)^2 + 4R\right]\sin^2\frac{\delta}{2}}{(1-R)^2 + 4R\sin^2\frac{\delta}{2}} \tag{8}$$

By defining $F = \frac{4R}{(1-R)^2}$, the phase difference is:

$$\delta = 2\arcsin\left(m\pi \pm \sqrt{\frac{\Delta}{1 + F(1-\Delta)}}\right) \tag{9}$$

By assuming that the light is normally incident to the thin film ($\theta' = 0$), $\delta = \frac{4\pi}{\lambda} n'h$ and $R = \frac{(n-1)^2}{(n+1)^2}$. Therefore, the film thickness can be computed from the normalized interference intensity as:

$$h = \frac{\lambda}{2\pi n'}\arcsin\left(m\pi \pm \sqrt{\frac{\Delta}{1 + F(1-\Delta)}}\right) \tag{10}$$

References

1. C. V. Boys, *Soap Bubbles: Their Colours and the Forces Which Mold Them*, Society for Promoting Christian Knowledge, London, 1912.

2. K. J. Mysels, S. Frankel and K. Shinoda, *Soap films: Studies of their Thinning and a Bibliography*, Pergamon Press, 1959.
3. E. Chatzigiannakis, N. Jaensson and J. Vermant, *Curr. Opin. Colloid Interface Sci.*, 2021, 101441.
4. P.-G. de Gennes and J. Badoz, *Fragile Objects: Soft Matter, Hard Science, and the Thrill of Discovery*, Springer-Verlag NewYork 1996.
5. I. Cantat, S. Cohen-Addad, F. Elias, F. Graner, R. Höhler and O. Pitois, *Foams: Structure and Dynamics*, Oxford University Press, Oxford, 2013.
6. M. Crne, V. Sharma, J. Blair, J. O. Park, C. J. Summers and M. Srinivasarao, *EPL (Europhysics Letters)*, 2011, **93**, 14001.
7. M. Srinivasarao, *Chem. Rev.*, 1999, **99**, 1935-1962.
8. Y. Zhang and V. Sharma, *Soft Matter*, 2015, **11**, 4408-4417.
9. Y. Zhang, S. Yilixiati, C. Pearsall and V. Sharma, *ACS Nano*, 2016, **10**, 4678-4683.
10. D. Langevin and A. A. Sonin, *Adv. Colloid Interface Sci.*, 1994, **51**, 1-27.
11. P. G. de Gennes, F. Brochard-Wyart and D. Quéré, *Capillarity and Wetting Phenomena: Drops, Bubbles, Pearls, Waves*, Springer-Verlag, New York, 2004.
12. R. I. Saye and J. A. Sethian, *Science*, 2013, **340**, 720-724.
13. D. L. Weaire and S. Hutzler, *The Physics of Foams*, Oxford University Press, Oxford, 1999.
14. G. Gochev, D. Platikanov and R. Miller, *Adv. Colloid Interface Sci.*, 2016, **233**, 115-125.
15. C. Hill and J. Eastoe, *Adv. Colloid Interface Sci.*, 2017, **247**, 496-513.
16. B. V. Derjaguin, N. V. Churaev and V. M. Muller, *Surface Forces*, Springer, New York, 1987.
17. V. Bergeron, *J. Phys.: Condens. Matter*, 1999, **11**, R215-R238.
18. S. Yilixiati, R. Rafiq, Y. Zhang and V. Sharma, *ACS Nano*, 2018, **12**, 1050-1061.
19. S. Yilixiati, E. Wojcik, Y. Zhang and V. Sharma, *Mol. Sys. Des. Eng.*, 2019, **4**, 626-638.
20. C. Ochoa, S. Gao, S. Srivastava and V. Sharma, *Proc. Natl. Acad. Sci. U.S.A.*, 2021, **118**, e2024805118.
21. C. Ochoa, C. Xu, C. D. M. Narváez, W. Yang, Y. Zhang and V. Sharma, *Soft Matter*, 2021, **17**, 8915-8924.
22. Y. Zhang and V. Sharma, *Langmuir*, 2018, **34**, 1208-1217.
23. Y. Zhang and V. Sharma, *Langmuir*, 2018, **34**, 7922–7931.
24. C. Ochoa, S. Gao, C. Xu, S. Srivastava and V. Sharma, *Soft Matter*, 2024, **20**, 1922-1934.
25. J. A. F. Plateau, *Statique expérimentale et théorique des liquides soumis aux seules forces moléculaires*, Gauthier-Villars, Paris, 1873.
26. K. J. Mysels, *The Journal of Physical Chemistry*, 1964, **68**, 3441-3448.
27. Y. Couder, J. M. Chomaz and M. Rabaud, *Physica D*, 1989, **37**, 384-405.
28. A. W. Reinold and A. W. Rucker, *Proc. R. Soc. London*, 1893, **53**, 394-398.
29. E. S. Johonnott, *Phil. Mag.*, 1906, **11**, 746-753.
30. J. Perrin, *Ann. Phys. (Paris)*, 1918, **10**, 160-184.
31. J. Perrin, in *Nobel Lectures, Physics 1922-1941*, Elsevier, Amsterdam, 1965.
32. F. Behroozi, *Am. J. Phys.*, 2008, **76**, 1087-1091.
33. J. C. C. Nitsche, *Am. Math. Monthly*, 1974, **81**, 945-968.
34. A. Sheludko, *Adv. Colloid Interface Sci.*, 1967, **1**, 391-464.

35. D. Dunmur and T. Sluckin, *Soap, science, and flat-screen TVs: a history of liquid crystals*, Oxford University Press, 2014.
36. P. Vorobieff and R. E. Ecke, *Am. J. Phys.*, 1999, **67**, 394-399.
37. E. Rio and A. L. Biance, *ChemPhysChem*, 2014, **15**, 3692-3707.
38. J. N. Israelachvili, *Intermolecular and Surface Forces*, Elsevier, Waltham, MA, 3rd edn., 2011.
39. A. D. Nikolov and D. T. Wasan, *J. Colloid Interface Sci.*, 1989, **133**, 1-12.
40. J. Lee, A. Nikolov and D. Wasan, *J. Colloid Interface Sci.*, 2017, **496**, 60-65.
41. J. Lee, A. D. Nikolov and D. T. Wasan, *J. Colloid Interface Sci.*, 2017, **487**, 217-222.
42. S. E. Anachkov, K. D. Danov, E. S. Basheva, P. A. Kralchevsky and K. P. Ananthapadmanabhan, *Adv. Colloid Interface Sci.*, 2012, **183**, 55-67.
43. K. D. Danov, E. S. Basheva, P. A. Kralchevsky, K. P. Ananthapadmanabhan and A. Lips, *Adv. Colloid Interface Sci.*, 2011, **168**, 50-70.
44. V. Bergeron and C. J. Radke, *Langmuir*, 1992, **8**, 3020-3026.
45. V. Bergeron, A. I. Jimenez-Laguna and C. J. Radke, *Langmuir*, 1992, **8**, 3027-3032.
46. O. Krichevsky and J. Stavans, *Phys. Rev. Lett.*, 1995, **74**, 2752.
47. R. Mukherjee and A. Sharma, *Soft Matter*, 2015, **11**, 8717-8740.
48. G. Reiter, *Phys. Rev. Lett.*, 1992, **68**, 75.
49. G. Reiter, S. Al Akhrass, M. Hamieh, P. Damman, S. Gabriele, T. Vilmin and E. Raphaël, *Eur. Phys. J.*, 2009, **166**, 165-172.
50. A. Sharma and G. Reiter, *J. Colloid Interface Sci.*, 1996, **178**, 383-399.
51. R. Seemann, S. Herminghaus and K. Jacobs, *Phys. Rev. Lett.*, 2001, **86**, 5534.
52. J. Becker, G. Grün, R. Seemann, H. Mantz, K. Jacobs, K. R. Mecke and R. Blossey, *Nat. Mater.*, 2003, **2**, 59-63.
53. S. Kalliadasis and U. Thiele, *Thin Films of Soft Matter*, SpringerWien NewYork, 2007.
54. V. C. Suja, M. Rodríguez-Hakim, J. Tajuelo and G. G. Fuller, *Adv. Colloid Interface Sci.*, 2020, **286**, 102295.
55. V. C. Suja, J. Sentmanat, G. Hofmann, C. Scales and G. G. Fuller, *Scientific reports*, 2020, **10**, 11378.
56. J. M. Frostad, D. Tammaro, L. Santollani, S. B. de Araujo and G. G. Fuller, *Soft Matter*, 2016, **12**, 9266-9279.
57. R. Cohen, D. Exerowa, T. Kolarov, T. Yamanaka and T. Tano, *Langmuir*, 1997, **13**, 3172-3176.
58. S. Sett, S. Sinha-Ray and A. L. Yarin, *Langmuir*, 2013, **29**, 4934-4947.
59. S. I. Karakashev, A. V. Nguyen and E. D. Manev, *J. Colloid Interface Sci.*, 2007, **306**, 449-453.
60. J. Seiwert, R. Kervil, S. Nou and I. Cantat, *Phys. Rev. Lett.*, 2017, **118**, 048001.
61. V. Ferraro, Z. Wang, L. Miccio and P. L. Maffettone, *J. Phys. Chem. C*, 2021, **125**, 1075-1086.
62. I. Krupka, R. Poliscuk, M. Liska, J. Molimard, M. Querry and P. Vergne, *Tribology Trans.*, 2001, **44**, 270-276.
63. C. Xu, C. D. V. Martínez Narváez, P. Kotwis and V. Sharma, *Langmuir*, 2023, **39**, 5761–5770.
64. S. I. Kemal, C. A. U. Ortiz and V. Sharma, *Mol. Sys. Des. Eng.*, 2021, **6**, 520-533.
65. S. Gao, C. Ochoa, V. Sharma and S. Srivastava, *Langmuir*, 2022, **38**, 11003-11014.

66. L. Hassan, C. Xu, M. Boehm, S. K. Baier and V. Sharma, *Langmuir*, 2023, **39**, 6102-6112.
67. P. J. Beltramo, R. Van Hooghten and J. Vermant, *Soft Matter*, 2016, **12**, 4324-4331.
68. P. J. Beltramo and J. Vermant, *ACS Omega*, 2016, **1**, 363-370.
69. J. P. King, R. R. Dagastine, J. D. Berry and R. F. Tabor, *J. Colloid Interface Sci.*, 2023.
70. A. D. Nikolov, P. A. Kralchevsky, I. B. Ivanov and D. T. Wasan, *J. Colloid Interface Sci.*, 1989, **133**, 13-22.
71. E. Shabalina, A. Bérut, M. Cavelier, A. Saint-Jalmes and I. Cantat, *Phys. Rev. Fluids*, 2019, **4**, 124001.
72. A. Gros, A. Bussonnière, S. Nath and I. Cantat, *Phys. Rev. Fluids*, 2021, **6**, 024004.
73. A. D. Nikolov and D. T. Wasan, *J. Colloid Interface Sci.*, 1989, **133**, 1-12.
74. P. Kralchevsky, A. Nikolov, D. T. Wasan and I. Ivanov, *Langmuir*, 1990, **6**, 1180-1189.
75. P. Heinig, C. M. Beltrán and D. Langevin, *Phys. Rev. E.*, 2006, **73**, 051607.
76. M. Ludwig and R. von Klitzing, *Curr. Opin. Colloid Interface Sci.*, 2020, **47**, 137-152.
77. L. Saulnier, L. Champougny, G. Bastien, F. Restagno, D. Langevin and E. Rio, *Soft Matter*, 2014, **10**, 2899-2906.
78. B. Scheid, J. Delacotte, B. Dollet, E. Rio, F. Restagno, E. A. van Nierop, I. Cantat, D. Langevin and H. A. Stone, *EPL*, 2010, **90**.
79. The protocols can be accessed at https://github.com/xcxery/IDIOM-Protocols